Exploring Event Camera-based Odometry for Planetary Robots

Florian Mahlknecht[1], Daniel Gehrig[2], Jeremy Nash[1], Friedrich M. Rockenbauer[1], Benjamin Morrell[1], Jeff Delaune[1] and Davide Scaramuzza[2]
[1] Jet Propulsion Laboratory, California Institute of Technology, USA
[2] Robotics and Perception Group, University of Zurich, Switzerland

***Abstract*— Due to their resilience to motion blur and high robustness in low-light and high dynamic range conditions, event cameras are poised to become enabling sensors for vision-based exploration on future Mars helicopter missions. However, existing event-based visual-inertial odometry (VIO) algorithms either suffer from high tracking errors or are brittle, since they cannot cope with significant depth uncertainties caused by an unforeseen loss of tracking or other effects. In this work, we introduce EKLT-VIO, which addresses both limitations by combining a state-of-the-art event-based frontend with a filter-based backend. This makes it both accurate and robust to uncertainties, outperforming event- and frame-based VIO algorithms on challenging benchmarks by 32%. In addition, we demonstrate accurate performance in hover-like conditions (outperforming existing event-based methods) as well as high robustness in newly collected Mars-like and high-dynamic-range sequences, where existing frame-based methods fail. In doing so, we show that event-based VIO is the way forward for vision-based exploration on Mars.**

Multimedia Material: For code and dataset please visit
`https://uzh-rpg.github.io/eklt-vio/`

I. Introduction

State estimation is critical for enabling autonomous navigation and control of mobile robots, with widespread applications from space exploration to household cleaning robots. There exist well-established algorithms, such as [1], [2], [3], [4] which estimate ego-motion from visual-inertial data. However, vision-based navigation is drastically impacted by the known limitations of conventional cameras, such as motion blur and low dynamic range.

Event cameras promise to address these limitations [5]. Unlike a standard camera that measures absolute pixel brightness using a global exposure time, event camera pixels independently detect positive or negative brightness changes at microsecond resolution. Event cameras can provide data at 1 MHz rate and 120 dB dynamic range, both orders of magnitude greater than what can be achieved with a standard 60 dB camera. This leads to a significant reduction in motion blur, and enables operation in high dynamic range (HDR), low light, and fast motion conditions [6], [7].

Part of this research was carried out at the Jet Propulsion Laboratory, California Institute of Technology, under a contract with the National Aeronautics and Space Administration. The other part of this work was carried out at the Robotics and Perception Group, University of Zurich, under contracts with the National Centre of Competence in Research (NCCR) Robotics through the Swiss National Science Foundation (SNSF) and the European Research Council (ERC) under grant agreement No. 51NF40_185543.

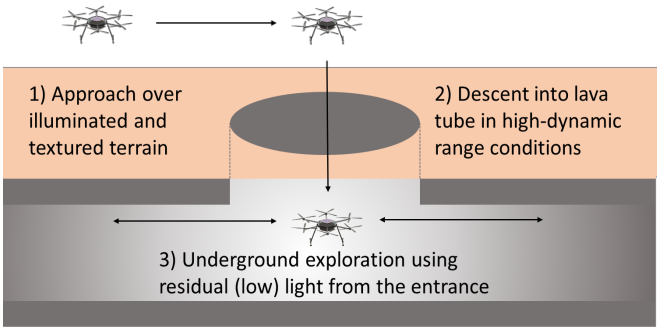

(a) Mission scenario

(b) Ingenuity Mars helicopter

(c) Lava tube

Fig. 1: New mission scenario (a) enabled by EKLT-VIO for a Mars helicopter (b) scouting the entrance of lava tubes (c).

On the application side, computer vision is increasingly used in modern planetary robotic missions [8], [9], [10], [11], [12], [13].The resilient properties of event cameras may enable robots to explore in conditions where frame cameras cannot operate without introducing the size, weight, power, and range limitations of a LiDAR.

In this paper, we focus on a scenario involving the exploration of the entrance of a lava tube by a Mars helicopter, as illustrated in Fig. 1. Lava tubes are natural tunnels created by lava flows in volcanic terrains. Those found on Mars have drawn significant attention because of the possibility that they might host microbial life [14]. The natural protection from radiation offered by lava tubes also makes them candidates to host the first human base on Mars.

Before sending a robotic mission [15] or astronauts to a specific lava tube, it would be desirable to scout and map several locations. Mars helicopters are candidate platforms to scout multiple lava tubes throughout a single mission. However, Mars helicopters cannot fly LiDARs and have to rely on passive cameras for navigation. Frame cameras are ill-suited to explore the lava tubes because of the HDR conditions created by the shadow at the entrance of the tube, as well as the low-light conditions once inside. This

capability gap is filled by event cameras, which offer the potential to explore and map the lava tube for potentially tens of meters using residual light from the entrance.

Mars helicopters come with their own requirements on the state estimation system [16], [10]. They must rely on small passive lightweight cameras to observe the full state up to scale and gravity direction. The camera is fused with an inertial measurement unit (IMU), which makes gravity observable, enables a high estimation rate, and acts as an emergency landing sensor in case of camera failure. Finally, a laser range finder is used to observe scale in the absence of accelerometer excitation. The estimation backend must be able to handle feature depth uncertainty associated with helicopter hovering and rotation-only dynamics. Typically, only filter-based approaches that estimate the variance of the depth can handle hovering robustly. This proved critical in Ingenuity Mars helicopter's sixth flight on Mars, where an image timestamping anomaly caused roll and pitch oscillations greater than 20 degrees [17]. Such out-of-plane rotations cause features to leave the camera field of view, which can lead to estimation failure in non-filter-based state estimation approaches, which are fundamentally unable to handle the depth uncertainty of the new feature tracks without a dedicated re-initialization procedure.

State-of-the-art event-based VIO methods are unsuitable in these conditions since they either are *(i)* optimization-based backends, which do not model depth uncertainty, thus featuring brittle performance in mission-typical rotation-only motion, or when a significant portion of features are lost [18], or *(ii)* show a higher tracking error, due to the use of suboptimal event-based frontends [19].

In this work, we introduce EKLT-VIO, which addresses the limitations above by *(i)* leveraging the event-based feature tracker EKLT [20]—which represents the current state-of-the-art in tracking accuracy for event-driven feature tracking—and *(ii)* combining it with an EKF backend that can handle pure rotational motion. EKLT-VIO is accurate, outperforming previous state-of-the-art frame-based and event-based methods on the challenging Event-Camera Dataset [21], with a 32% improvement in terms of pose accuracy. Moreover, it can handle purely-rotational motion tracking robustly and accurately, while existing optimization-based methods fail to initialize. This is because they require lengthy bootstrapping sequences, which would be impractical on Mars. Additionally, it maintains state-estimate, even when frame-based methods fail due to excessive motion blur. We showcase the advantages of the event-based EKLT frontend in newly collected Mars-like conditions, showing better tracking performance than existing methods. This demonstrates the viability of our EKLT-VIO on Mars. Our contributions are the following:

- We introduce EKLT-VIO, an event-based VIO method that combines an accurate state-of-the-art event-based feature tracker EKLT with an EKF backend. It outperforms state-of-the-art event- and frame-based methods, reducing the overall tracking error by 32%.
- We show accurate and robust tracking even in rotation-only sequences, which are closest to the hover-like scenarios experienced by Mars helicopters, outperforming optimization-based and frame-based methods.
- We outperform existing methods on newly collected Mars-like sequences collected in the JPL Mars Yard and Wells Cave for planetary exploration.

II. Related Work

Visual-inertial odometry has been well-studied over the past years. While traditionally, standard cameras and IMUs were used, more recently, an emerging line of work has exploited the advantages of event cameras.

A. Frame-based VIO

An overview of existing approaches is discussed in [22]. Frame-based VIO algorithms can be roughly segmented into two classes: optimization-based and filter-based algorithms [22]. While both algorithms focus on tracking camera poses by minimizing both visual and inertial residuals, optimization-based methods solve this by performing iterative Gauss-Newton steps, while filtering-based methods achieve this through Kalman Filtering steps.

Due to the costly nature of optimizing both 3D landmarks (*i.e.*, SLAM features) and camera poses, several filtering-based techniques exist that focus on refining camera poses from bearing measurements (*i.e.*, multi-state constraint Kalman filter (MSCKF) features [23]) directly. While these techniques are more efficient, they need translational motion and provide updates only after the full feature track is known. A recent filtering-based approach, xVIO [16], combines the advantages of both types of features, with robustness to depth uncertainty in rotation-only motion and computational efficiency with many MSCKF features.

B. Event-based VIO

While event cameras were first introduced in 2008 [24], the first event-based, 6-DOF visual odometry (VO) algorithms only started to appear recently [25], [26]. Later work incorporated an IMU to improve tracking performance and stability [27], [19], achieving impressive tracking on a fast spinning leash [27]. Despite their robustness, these methods are not immune to drift due to the differential nature of the used sensors. For this reason, most recently, Ultimate SLAM (USLAM) [18] used a combination of events, frames, and IMU, all provided by the Dynamic and Active Vision Sensor (DAVIS) [28]. It tracks FAST corners [29] on frames and motion-compensated event frames separately using the Lucas-Kanade tracker (KLT) [30] and fuses these feature tracks with IMU measurements in a sliding window.

While addressing drift, USLAM still relies on a sliding window optimization scheme, which is expensive and does not allow pose-only optimization through the use of MSCKF features. Moreover, its FAST/KLT frontend, first introduced in [27], is optimized explicitly for frame-like inputs and was shown to transfer suboptimally to event-based frames [20]. In this work, we incorporate the state-of-the-art event-based tracker EKLT [20], which takes a more principled approach

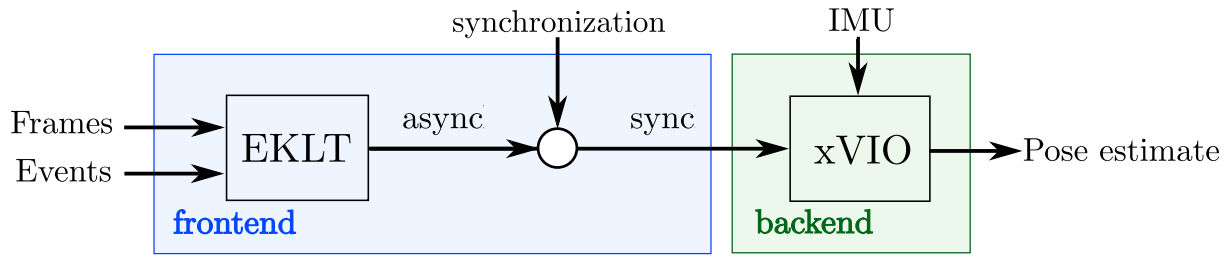

Fig. 2: We combine the state-of-the-art feature tracker, EKLT, which leverages frames and events, with the filter-based backend xVIO to enable hover-like, low-translation state-estimation. In contrast to standard, frame-based VIO, an additional user-defined synchronization step turns asynchronous feature tracks to synchronous matches, which are used by the backend. This enables variable-rate backend updates.

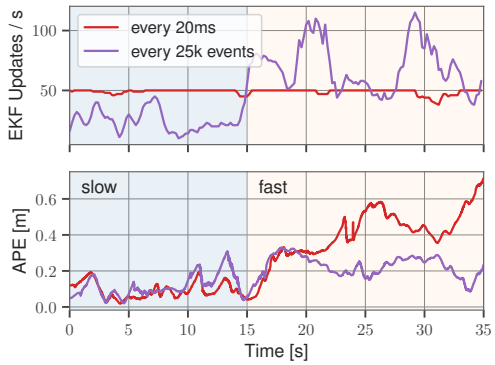

Fig. 3: Asynchronous EKF update strategy comparison. Synchronous feature updates (red) tend to generate too many updates during slow sequences and too few during fast sequences, leading to high tracking error. Our irregular update strategy (purple) adapts to the event-rate, and thus maintains low tracking error in both scenarios.

to fusing events and frames, and thus achieves better feature tracking performance compared to [18], [27].

III. Methodology

In this section we present EKLT-VIO, which is illustrated in Fig. 2. It is an event-based VIO algorithm based on the state-of-the-art event tracker EKLT, coupled with a filter-based xVIO backend. We start by providing a summary of the xVIO backend. For more details see [16].

A. Backend

xVIO: The backend fuses data from an inertial measurement unit (IMU) and feature tracks from the frontend. It does this by using an extended Kalman filter (EKF) with an IMU state $\mathbf{x}_I$ and a visual state $\mathbf{x}_V$:

$$\mathbf{x} = \begin{bmatrix}\mathbf{x}_I{}^\intercal & \mathbf{x}_V{}^\intercal\end{bmatrix}^\intercal \tag{1}$$

The IMU state follows an inertial propagation scheme as described in [31]. The visual state $\mathbf{x}_V$ is split into sliding window states $\mathbf{x}_S$ and feature states $\mathbf{x}_F$:

$$\mathbf{x}_V = \begin{bmatrix}\mathbf{x}_S{}^\intercal & \mathbf{x}_F{}^\intercal\end{bmatrix}^\intercal \tag{2}$$

$$\mathbf{x}_S = \begin{bmatrix}\mathbf{p}_w^{c_1}{}^\intercal & \dots & \mathbf{p}_w^{c_M}{}^\intercal & \mathbf{q}_w^{c_1}{}^\intercal & \dots & \mathbf{q}_w^{c_M}{}^\intercal\end{bmatrix}^\intercal \tag{3}$$

$$\mathbf{x}_F = \begin{bmatrix}\mathbf{f}_1 & \dots & \mathbf{f}_N\end{bmatrix}^\intercal \tag{4}$$

The sliding window states contain the positions, $\mathbf{p}_w^{c_i}$, and attitudes parameterized as quaternions, $\mathbf{q}_w^{c_i}$, of the last M camera poses $\{c_i\}$ with respect to a world frame $\{w\}$. The feature states contain the 3D positions, $\mathbf{f}_j$, of N SLAM features. In this work $N = 15$ and $M = 10$.

SLAM features are parametrized with respect to an anchor pose $\mathbf{p}_w^{c_{a_j}}$ in the sliding window and are defined as follows:

$$\mathbf{f}_j = \begin{bmatrix}\alpha_j & \beta_j & \rho_j\end{bmatrix} \tag{5}$$

with α_j and β_j being normalized image coordinates and ρ_j being the inverse depth. Each time the feature tracks are updated, each SLAM feature j is converted from inverse-depth to Cartesian coordinates in the associated anchor camera frame $\{c_{a_j}\}$.

$$\mathbf{p}_{c_i}^j = \mathbf{C}(\mathbf{q}_w^{c_i})\left(\mathbf{p}_w^{c_{a_j}} + \frac{1}{\rho_j}\mathbf{C}(\mathbf{q}_w^{c_{a_j}})^\intercal\begin{bmatrix}\alpha_j\\ \beta_j\\ 1\end{bmatrix} - \mathbf{p}_w^{c_i}\right), \tag{6}$$

The measurement model is the normalized feature:

$$\mathbf{z}_j = \pi(\mathbf{p}_{c_i}^j) + \mathbf{n}_j, \quad \pi(\mathbf{x}) = \frac{1}{x_3}\begin{bmatrix}x_1\\ x_2\end{bmatrix}, \tag{7}$$

where $\pi(\mathbf{x})$ performs feature projection, $\mathbf{n}_j$ is Gaussian noise, and $\mathbf{z}_j$ are the new feature observations by the frontend, expressed in normalized image coordinates. Eqs. (6) and (7) can be used to develop the EKF update by linearizing the SLAM feature reprojection. Details are given in [16].

In addition to SLAM features, the backend maintains MSCKF features that additionally constrain the camera poses without an explicit inverse depth. MSCKF features are thus not part of the state, resulting in a smaller computational cost per feature. They need to be observed for the last $2 \leq m \leq M$ frames, providing a corresponding observation for each pose in the sliding window. MSCKF features

require triangulation using those pose priors, so they can only be processed once a track with significant translation is observed. We discard features if a minimum translation threshold is not exceeded. In the next section, we describe the event-based frontend used to provide feature observations.

B. Frontend

We base our frontend on the state-of-the-art event- and frame-based feature tracker EKLT. While we provide a summary of EKLT here, more details can be found in [20].

EKLT: EKLT tracks Harris corners, extracted on frames, by aligning the predicted and measured brightness increment in a patch around the corners. It minimizes the normalized distance between these patches to recover the warping parameters $\mathbf{p}$ and normalize optical flow $\mathbf{v}$ as

$$\{\mathbf{p}, \mathbf{v}\} = \arg\min_{\mathbf{p},\mathbf{v}} \left\| \frac{\Delta L(\mathbf{u})}{\|\Delta L(\mathbf{u})\|} - \frac{\Delta \hat{L}(\mathbf{u}, \mathbf{p}, \mathbf{v})}{\left\|\Delta \hat{L}(\mathbf{u}, \mathbf{p}, \mathbf{v})\right\|} \right\|. \quad (8)$$

While ΔL is defined as an aggregation of events in a local patch, $\Delta \hat{L}$ is defined as the negative dot product between the local log image gradient and optical flow vector, following the linearized event generation model [32]:

$$\Delta \hat{L}(\mathbf{u}, \mathbf{p}, \mathbf{v}) = -\nabla \hat{L}(\mathbf{W}(\mathbf{u}, \mathbf{p})) \cdot \mathbf{v} \Delta t \quad (9)$$

Here $W(\mathbf{u}, \mathbf{p})$ aligns the image gradient with the measured brightness increments according to the alignment parameters p. By minimizing Eq. (8), these alignment parameters p and optical flow v are found. As opposed to the reference implementation of EKLT, which optimizes in a sliding window fashion after a fixed number of events, we trigger the optimization only when the adaptive number of events is reached, using each event batch only once. This entails a significant speed-up without loss in accuracy.

The following section discusses additional innovation to combine the above features trackers with xVIO and the pursued outlier rejection strategy.

C. Frontend Adaptations

Asynchronous feature updates: We convert the asynchronous feature tracks provided by EKLT to synchronous feature tracks via a synchronization step (Fig. 2. This step produces a temporally synchronized list of feature positions, which are passed to the backend. The backend uses the associated correspondences $\mathbf{z}_i \iff \mathbf{z}_j$ together with consecutive camera poses c_i and c_j to update the state as discussed in Sec. III-A. It is performed by selecting the most recent feature in the currently tracked feature set and extrapolating the positions of all other features to its timestamp. We synchronize every time, a fixed number of events n is triggered, enabling variable-rate backend updates. We empirically found $n = 3200$ to work best. This variable rate allows our algorithm to adapt to the scene dynamics (Fig. 3), leading to fewer EKF updates in slow sequences (Fig.3, left) while having a lower tracking error during high-speed sequences, than when using a fixed rate. These features motivate the use of an event-based frontend since a purely frame-based one is limited by the framerate of the camera.

Outlier rejection: For EKLT we exclusively reject outliers by setting a maximum threshold on the optimized residual of the alignment score in Eq. (8). This allows outliers to be rejected quickly, without the need for costly geometric verification, such as 8-point RANSAC.

IV. Experiments

We start by validating our approach on standard benchmarks in Sec. IV-B, where we compare the performance of EKLT-VIO against state-of-the-art event-based [19], frame-based [16] and event- and frame-based methods [18]. To study the effect on the event-based feature tracker, we also study an additional baseline, based on the HASTE feature tracker [33]. We then proceed to demonstrate the suitability of our approach on two important use-cases motivated by the Mars exploration scenario: *(i)* pure rotational motion, imitating hover-like conditions on Mars (Sec. IV-C), and *(ii)* challenging HDR conditions on newly collected datasets in the JPL Mars Yard and at the entrance of the Wells Cave, emulating the entry into lava tubes (Sec. IV-D).

A. Baselines and Compared Methods

USLAM [18] is an event- and frame-based VIO method, which fuses feature tracks derived from frames and event-frames in an optimization-based backend.
EVIO [19] uses only events and IMU. Events are used to generate asynchronous feature tracks, which are then fused in a filter-based backend. Since open-source code is not available, we only report results on real sequences.
KLT-VIO [16] is a frame-based VIO method that fuses feature tracks based on FAST/KLT in a filter-based backend, and is specifically designed for use during helicopter flight.
HASTE-VIO [33] Finally, to study the effect of event-based frontends, we implement an additional baseline, based on the state-of-the-art purely event-based feature tracker HASTE [33]. Similar to EKLT, it produces asynchronous feature tracks which are first synchronized using the method described in Sec. III-C, before being fed into the backend.

B. Real Data

As a next step, we benchmark our methods on the Event-Camera Dataset [21]. This dataset is set in an office environment and was recorded with a DAVIS 240C [28], which provides synchronized images, events, IMU measurements. An OptiTrack is used for ground-truth camera trajectories. The sequences in this dataset feature very fast hand-held motions in an HDR scenario. Next to the common translation and 6DOF motion sequences, we also evaluate on the rotation-only sequences which more closely mimic the hover-like scenarios we are addressing. We evaluate the pose tracking accuracy using the same protocol as [18], and report mean position error (MPE) in % of the total trajectory length

Dataset	USLAM* [18]		USLAM [18]		EVIO [19]		KLT-VIO [16]		HASTE-VIO		EKLT-VIO (**ours**)	
	MPE	MYE	MPE	MYE	MPE	MYE	MPE	MYE	MPE	MYE	MPE	MYE
Boxes 6DOF	0.30	0.04	**0.68**	**0.03**	4.13	0.92	0.97	0.05	2.03	**0.03**	0.84	0.09
Boxes Translation	0.27	0.02	1.12	2.62	3.18	0.67	**0.33**	**0.08**	2.55	0.46	0.48	0.25
Dynamic 6DOF	0.19	0.10	0.76	0.09	3.38	1.20	0.78	**0.03**	**0.52**	0.06	0.79	0.06
Dynamic Translation	0.18	0.15	0.63	0.22	1.06	0.25	0.55	0.06	1.32	0.06	**0.40**	**0.04**
HDR Boxes	0.37	0.03	1.01	0.31	3.22	0.15	**0.42**	**0.02**	1.75	0.09	0.46	0.06
HDR Poster	0.31	0.05	1.48	0.09	1.41	0.13	0.77	0.03	0.57	**0.02**	**0.65**	0.04
Poster 6DOF	0.28	0.07	0.59	0.03	5.79	1.84	0.69	**0.02**	1.50	0.03	**0.35**	**0.02**
Poster Translation	0.12	0.04	0.24	**0.02**	1.59	0.38	**0.16**	**0.02**	1.34	**0.02**	0.35	0.03
Shapes 6DOF	0.10	0.04	1.07	0.03	2.52	0.61	1.80	0.03	2.35	**0.02**	**0.60**	0.03
Shapes Translation	0.26	0.06	1.36	**0.01**	4.56	2.60	1.38	0.02	1.09	0.02	**0.51**	0.03
Average	0.24	0.06	0.89	0.34	3.08	0.88	0.79	**0.04**	1.50	0.08	**0.54**	0.07

*per-sequence hyperparameter tuning and correct IMU bias intialization

TABLE I: Pose estimate accuracy comparison on the Event-Camera Dataset [21] in terms of mean position error (MPE) in % and mean yaw error (MYE) in deg/m. Grayed-out results with (*) by USLAM [18] were achieved through per-sequence parameter tuning and correct IMU bias initialization, while results in black used a single parameter set, tuned on all sequences simultaneously, and were initialized with an IMU bias of zero.

Dataset	USLAM [18]		KLT-VIO [16]		HASTE-VIO		EKLT-VIO (**ours**)	
	MPE	MYE	MPE	MYE	MPE	MYE	MPE	MYE
Dynamic Rotation	*unfeasible*		9.97	**0.13**	**6.22**	2.32	7.71	1.52
Boxes Rotation			*diverging*		20.57	**1.32**	**8.78**	1.36
Poster Rotation			*diverging*		3.96	**0.09**	**1.44**	**0.09**
Shapes Rotation			*diverging*		*diverging*		**6.95**	**4.59**

TABLE II: Pose estimation accuracy in terms of mean position error (MPE) in % and mean yaw error (MYE) in deg/m on rotation-only sequences.

and mean yaw error (MYE) in deg/m in Tab.I. Additionally, we report results by KLT-VIO [16] and USLAM [18].

In [18], USLAM uses different parameters for each sequence, as well as correct IMU bias initialization, resulting in the gray columns in Tab. I. We mark this method as USLAM*. However, on Mars, a VIO system is expected to perform robustly in unknown environments, and thus, parameter tuning and bias initialization is not an option. For this reason, we retune the parameters of USLAM to perform best on all sequences simultaneously resulting in the black values in Tab. I. All other methods were tuned in the same way. Comparing USLAM* with USLAM shows that IMU bias initialization, and per-sequence hyperparameter tuning are clearly important to achieve low tracking error, reducing the error from 0.89% to 0.24%. Our EKLT-VIO, on the other hand, achieves an average error of 0.54% without bias initialization, 39% lower than USLAM. This improvement indicates that EKLT-VIO is simultaneously more robust to zero IMU bias initialization, and per-sequence hyperparameter tuning.

In terms of position error, EKLT-VIO outperforms all other methods on 5 out of 10 sequences. With an average MPE of 0.54% EKLT-VIO shows a 32% lower MPE than runner-up KLT-VIO with 0.79%. Finally, with a 3.08% MPE, EVIO [19] is outperformed by EKLT-VIO by 82%.

C. Rotation-only sequences

As shown in the previous sections, EKLT-VIO achieves significantly lower tracking error compared to the state-of-the-art methods, and the HASTE-VIO baseline. As a next step, we show the suitability of EKLT-VIO in a Mars Mission-like scenario. To do this, we evaluate all methods on the rotation-only sequences of the Event-Camera Dataset, which are challenging for optimization-based backends such as USLAM [18]. Similar to hover-like conditions expected during Mars missions, these sequences translate only little compared to the average scene depth, which poses a challenge for keyframe generation and triangulation.

We adopt the same evaluation protocol as before and report results for all methods in Tab. II. We observed during this experiment that USLAM did not initialize during these sequences since it could never detect sufficient translation to insert a new keyframe, and it is thus marked with *unfeasible*. Frame-based KLT-VIO manages to provide a non-diverging state estimate for the first 30s in the 60s long sequences. In the second part, however, shaking motion causes motion blur on the frames, making it impossible to produce accurate feature tracks, leading to a diverging state estimate. By contrast, event-based methods EKLT-VIO and HASTE-VIO can track robustly, because their event-based front-ends are unaffected by motion-blur. EKLT-VIO, however, is the only method to converge on all sequences and yields a consistently

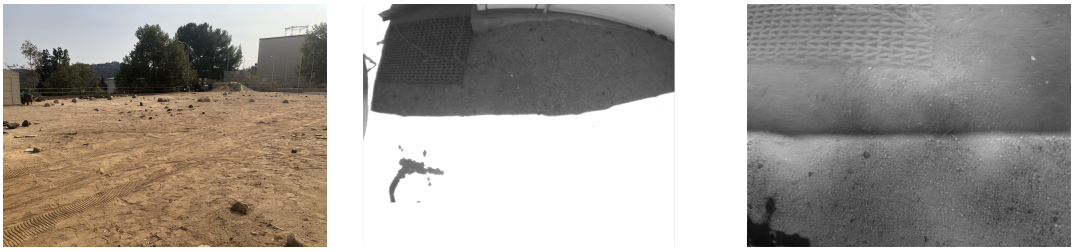

(a) Mars Yard preview (b) Overexposed image (c) Image reconstructed from events

(d) Wells Cave preview (e) Underexposed image (f) Image reconstructed from events

Fig. 4: Overview of the Mars Yard (a) and Wells Cave (d). In the Mars Yard, we test HDR conditions which cause severe oversaturation artefacts in standard images (b). Instead, in the Wells Cave we study the low light scenario encountered in lava tubes, which cause undersaturation (e). HDR images reconstructed from events [34] (c,f) do not suffer from these artefacts, and are used by our method.

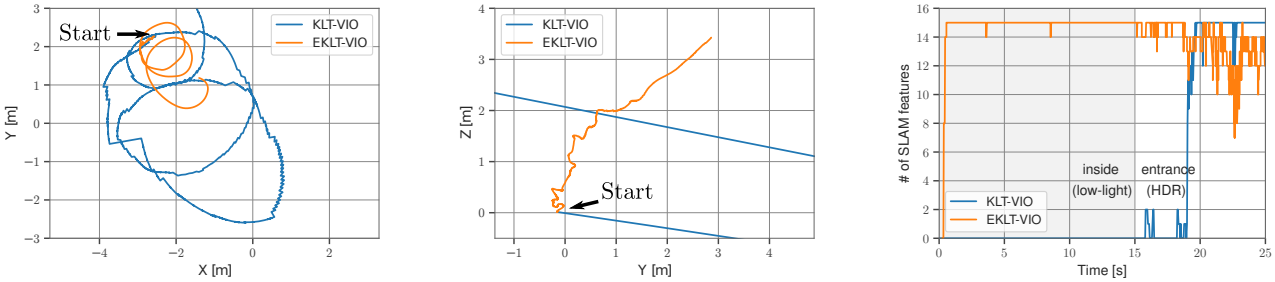

(a) Mars Yard (b) Wells Cave (c) Num Features Tracked in Wells Cave

Fig. 5: Trajectory comparison between EKLT-VIO (orange) and KLT-VIO (blue) in the Mars Yard (a) and Wells Cave (b). While KLT-VIO quickly diverges, due to a lack of tracked features (c), EKLT-VIO can track successfully.

lower tracking error compared to all compared methods. In summary, EKLT-VIO can leverage the advantages of an event-based frontend for robust tracking at high speeds and the advantages of a filter-based backend to fuse small translational motion into a consistent pose estimate. This shows that EKLT-VIO is most suitable in these conditions.

D. Mars-mission Scenario: Wells Cave and JPL Mars yard

Finally, to showcase the capabilities of EKLT-VIO in Mars-like exploration scenarios, we compare our method against KLT-VIO using standard images on sequences recorded at the JPL Mars Yard (Fig. 4 (a)), and Wells Cave Nature Preserve (Fig. 4 (d)). The Mars Yard features rapid changes in illumination conditions, which cause autoexposure to fail, and results in frequent overexposures in the images (Fig. 4 (d)), which are detrimental for image-based frontends. The Wells Cave instead is a cave system used by JPL to emulate lava tube environments observed on Mars. It features a low illumination, leading to underexposure in the images (Fig. 4 (d)). We collect sequences using the DAVIS 346[35] in the Wells Cave, and a different sensor setup consisting of one standard camera (mvBlueFOX-MLC200wG), one event camera (DVXplorer), and one IMU (MPU9250) in the Mars Yard.

In this scenario, we show that EKLT-VIO can run independently of standard frames. To do this we rely on images reconstructed from events, by the method E2VID [34]. They feature a much higher dynamic range than the standard images (Fig. 4 (f)). We reconstruct frames after every 15'000 events, resulting in an HDR video used by our method.

Mars Yard: The trajectory used in this analysis is a hand-held circular motion with a diameter of 1.5 meters over a sharp shadow with increasing speed. The trajectories tracked by KLT-VIO and EKLT-VIO are shown in Fig. 5 (a). While EKLT-VIO consistently tracks the circular motion for at least 2 revolutions, KLT-VIO diverges, due to a lack of features.

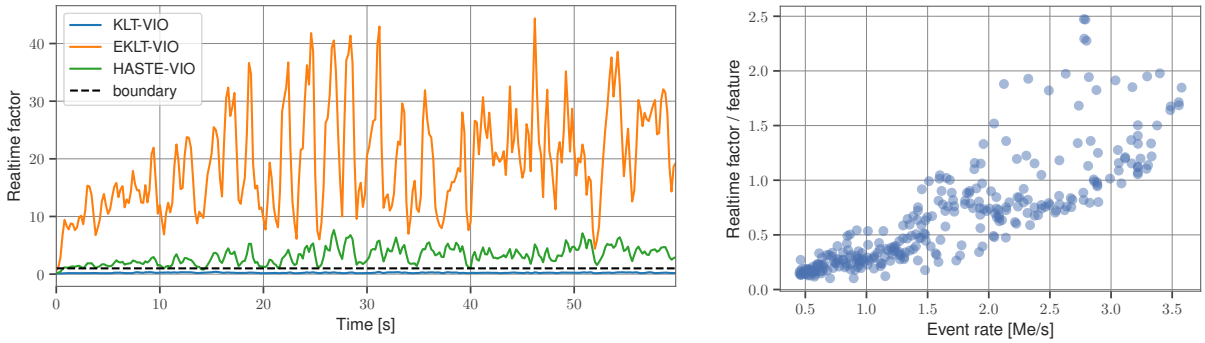

(a) Realtime factor (b) Realtime factor vs. Event rate

Fig. 6: Realtime factor (a) for EKLT-VIO (orange), HASTE-VIO (green) and KLT-VIO (blue) on the *Poster 6DOF* sequence. A real-time factor below 1 means the algorithm can process the data in real-time. The computational computational requirements of our method depends on the event rate. As seen in (b) The real-time factor per tracked feature correlates super-linearly with the event rate.

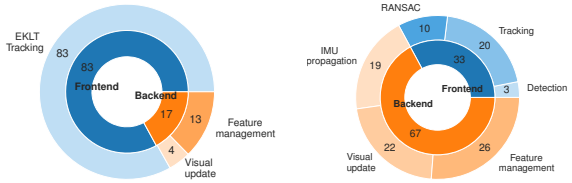

(a) EKLT-VIO (ours) (b) KLT-VIO

Fig. 7: Relative computation time spent by EKLT-VIO (a) and KLT-VIO [16] (b). The main bottleneck in EKLT-VIO is the feature tracker. By contrast, KLT-VIO spends most of its time in the backend.

This shows that thanks to the use of an event-based frontend EKLT-VIO can overcome this challenging condition.

Wells Cave: Finally, we test our method in the Wells Cave. The trajectories of KLT-VIO, and EKLT-VIO are shown in Fig. 5. While KLT-VIO diverges, EKLT-VIO tracks consistently, until the entrance of the tunnel is reached. EKLT-VIO manages to consistently maintain SLAM features, while KLT-VIO does not have any, as shown in Fig. 5. As soon as the camera exits the cave, KLT-VIO recovers.

E. Limitations

Computational Performance: We study EKLT-VIO, KLT-VIO, and HASTE-VIO in terms of their real-time factor (Fig. 6) and computation allocations (Fig. 7), and conduct all our experiments on a laptop with an Intel i7-7700HQ quadcore processor. The real-time factor (Fig. 6) measures how much computation time is spent to process a second of real-time, and a factor below 1 indicates that the algorithm is real-time capable. As seen in Fig. 6 (a) there exists a clear speed-accuracy trade-off between EKLT-VIO, HASTE-VIO, and KLT-VIO, since EKLT-VIO achieves a maximum real-time factor of around 45. For EKLT-VIO, the real-time factor correlates with the event rate (Fig. 6 (b)), which depends on the scene texture and camera speed.

As indicated in Fig.7, the EKLT frontend remains the bottleneck, which directs future work toward speeding up EKLT. Possible solutions include providing an initial estimate for the optimization by exploiting IMU information and distributing computation over multiple cores.

Interestingly, EKLT-VIO also has a higher backend utilization than KLT-VIO since it has a higher update rate, leading to frequent reparametrizations of the inverse-depth features for a given siding-window size.

Further optimizations: These include exploiting the fully asynchronous nature of the frontend by asynchronously triggering EKF updates, each time a feature is updated. To reduce computation, the feature states should be managed in a way that reduces the number of reparametrizations needed. This could be achieved by either switching from an inverse-depth to a Cartesian representation, or by sliding the pose window using a spatial criterion instead of a time criterion.

V. Conclusion

In light of future planetary missions, novel algorithms must be developed to handle the challenging lighting conditions and motions expected on Mars. Event cameras promise to enable these missions through their inherently robust perception. In this work, we present EKLT-VIO which exploits these superior properties of event cameras for visual-inertial odometry. It integrate the state-of-the-art asynchronous feature tracker EKLT with the filter-based backend xVIO thus leveraging both advantages. On the one hand, the event-based frontend provides high-speed feature measurements, which are robust in visually challenging scenarios such as high-speed, low light, and high dynamic range. On the other hand, the filter-based backend addresses the limitations of traditional optimization-based VIO algorithms in near-hovering conditions where keyframes cannot be selected due to a lack of translation. We show an evaluation on Mars-like sequences and challenging hand-held sequences of the Event-Camera dataset. On these sequences, we demonstrate the robust pose

tracking the performance of our methods, showing a mean position error reduction of up to 32% compared to event- and frame-based state-of-the-art methods. Additionally, we showcase the advantages of both backend and frontend in the first successful evaluation on the rotation-only sequences of the Event-Camera Dataset with fast motion and challenging lighting conditions. Finally, we demonstrate our method's robustness in visually challenging conditions recorded in the JPL Mars Yard and in the Wells Cave, replicating our mission scenario. To spur further research in this direction, we provide an open-source implementation of this work and release our Mars-like sequences upon acceptance.

REFERENCES

[1] M. Li and A. I. Mourikis, "Optimization-based estimator design for vision-aided inertial navigation," in *Robotics: Science and Systems*. Berlin Germany, 2013, pp. 241–248.

[2] S. Leutenegger, S. Lynen, M. Bosse, R. Siegwart, and P. Furgale, "Keyframe-based visual-inertial SLAM using nonlinear optimization," *Int. J. Robot. Research*, 2015.

[3] T. Qin, P. Li, and S. Shen, "VINS-Mono: A robust and versatile monocular visual-inertial state estimator," *IEEE Trans. Robot.*, vol. 34, no. 4, pp. 1004–1020, 2018.

[4] C. Forster, L. Carlone, F. Dellaert, and D. Scaramuzza, "On-manifold preintegration for real-time visual–inertial odometry," *IEEE Transactions on Robotics*, vol. 33, no. 1, pp. 1–21, 2016.

[5] G. Gallego, T. Delbruck, G. Orchard, C. Bartolozzi, B. Taba, A. Censi, S. Leutenegger, A. Davison, J. Conradt, K. Daniilidis, and D. Scaramuzza, "Event-based vision: A survey," *IEEE Trans. Pattern Anal. Mach. Intell.*, 2020.

[6] A. Rosinol Vidal, H. Rebecq, T. Horstschaefer, and D. Scaramuzza, "Ultimate SLAM? combining events, images, and IMU for robust visual SLAM in HDR and high speed scenarios," *IEEE Robot. Autom. Lett.*, vol. 3, no. 2, pp. 994–1001, Apr. 2018.

[7] S. Sun, G. Cioffi, C. De Visser, and D. Scaramuzza, "Autonomous quadrotor flight despite rotor failure with onboard vision sensors: Frames vs. events," *IEEE Robotics and Automation Letters*, vol. 6, no. 2, pp. 580–587, 2021.

[8] A. Johnson, S. Aaron, J. Chang, Y. Cheng, J. Montgomery, S. Mohan, S. Schroeder, B. Tweddle, N. Trawny, and J. Zheng, "The lander vision system for Mars 2020 entry descent and landing," in *AAS Guidance, Navigation, and Control Conference*, 2017.

[9] B. Bos, M. Ravine, M. Caplinger, J. Schaffner, J. Ladewig, R. Olds, C. Norman, D. Huish, M. Hughes, S. Anderson, D. Lorenz, A. May, C. Adam, D. Nelson, M. Moreau, D. Kubitschek, K. Getzandanner, K. Gordon, A. Eberhardt, and D. Lauretta, "Touch and go camera system (TAGCAMS) for the OSIRIS-REx asteroid sample return mission," *Space Science Reviews*, vol. 214, 01 2018.

[10] D. S. Bayard, D. T. Conway, R. Brockers, J. H. Delaune, L. H. Matthies, H. F. Grip, G. B. Merewether, T. L. Brown, and A. M. San Martin, "Vision-based navigation for the NASA Mars helicopter," in *AIAA Scitech 2019 Forum*, 2019, p. 1411.

[11] M. Maimone, Y. Cheng, and L. Matthies, "Two years of visual odometry on the Mars exploration rovers," *J. Field Robot.*, vol. 24, no. 3, pp. 169–186, 2007.

[12] J. Bapst, T. J. Parker, J. Balaram, T. Tzanetos, L. H. Matthies, C. D. Edwards, A. Freeman, S. Withrow-Maser, W. Johnson, E. Amador-French, J. L. Bishop, I. J. Daubar, C. M. Dundas, A. A. Fraeman, C. W. Hamilton, C. Hardgrove, B. Horgan, C. W. Leung, Y. Lin, A. Mittelholz, and B. P. Weiss, "Mars Science Helicopter: Compelling Science Enabled by an Aerial Platform," in *Bulletin of the American Astronomical Society*, vol. 53, May 2021, p. 361.

[13] J. Delaune, R. Brockers, D. S. Bayard, H. Dor, R. Hewitt, J. Sawoniewicz, G. Kubiak, T. Tzanetos, L. Matthies, and J. Balaram, "Extended navigation capabilities for a future mars science helicopter concept," in *IEEE Aerospace Conference*, 2020, pp. 1–10.

[14] B. Carrier, D. Beaty, M. Meyer, J. Blank, L. Chou, S. DasSarma, D. Des Marais, J. Eigenbrode, N. Grefenstette, N. Lanza, A. Schuerger, P. Schwendner, H. Smith, C. Stoker, J. Tarnas, K. Webster, C. Bakermans, B. Baxter, M. Bell, and J. G. Xu, "Mars extant life: What's next? conference report," *Astrobiology*, vol. 20, 05 2020.

[15] C. Phillips-Lander, J. Wynne, N. Chanover, C. Demirel-Floyd, K. Uckert, K. Williams, T. Titus, J. Blank, P. Boston, K. Mitchell, D. Wyrick, S. Shkolyar, K. Retherford, and F. J. Martín-Torres, "Mars astrobiological cave and internal habitability explorer (MACIE): A new frontiers mission concept," in *38th Mars Exploration Program Analysis Group*, 04 2020.

[16] J. Delaune, D. S. Bayard, and R. Brockers, "Range-visual-inertial odometry: Scale observability without excitation," *IEEE Robotics and Automation Letters*, vol. 6, no. 2, pp. 2421–2428, 2021.

[17] H. Grip, "Surviving an In-Flight Anomaly: What Happened on Ingenuity's Sixth Flight," NASA, Tech. Rep., 2021.

[18] A. R. Vidal, H. Rebecq, T. Horstschaefer, and D. Scaramuzza, "Ultimate slam? combining events, images, and imu for robust visual slam in hdr and high-speed scenarios," *IEEE Robotics and Automation Letters*, vol. 3, no. 2, pp. 994–1001, 2018.

[19] A. Z. Zhu, N. Atanasov, and K. Daniilidis, "Event-based visual inertial odometry," in *IEEE Conf. Comput. Vis. Pattern Recog. (CVPR)*, 2017, pp. 5816–5824.

[20] D. Gehrig, H. Rebecq, G. Gallego, and D. Scaramuzza, "EKLT: Asynchronous photometric feature tracking using events and frames," *Int. J. Comput. Vis.*, 2019.

[21] E. Mueggler, H. Rebecq, G. Gallego, T. Delbruck, and D. Scaramuzza, "The event-camera dataset and simulator: Event-based data for pose estimation, visual odometry, and SLAM," *Int. J. Robot. Research*, vol. 36, no. 2, pp. 142–149, 2017.

[22] J. Delmerico and D. Scaramuzza, "A benchmark comparison of monocular visual-inertial odometry algorithms for flying robots," in *IEEE Int. Conf. Robot. Autom. (ICRA)*, 2018.

[23] A. I. Mourikis and S. I. Roumeliotis, "A multi-state constraint Kalman filter for vision-aided inertial navigation," in *IEEE Int. Conf. Robot. Autom. (ICRA)*, 2007, pp. 3565–3572.

[24] P. Lichtsteiner, C. Posch, and T. Delbruck, "A 128×128 120 dB 15 μs latency asynchronous temporal contrast vision sensor," *IEEE J. Solid-State Circuits*, vol. 43, no. 2, pp. 566–576, 2008.

[25] H. Kim, S. Leutenegger, and A. J. Davison, "Real-time 3D reconstruction and 6-DoF tracking with an event camera," in *Eur. Conf. Comput. Vis. (ECCV)*, 2016, pp. 349–364.

[26] H. Rebecq, T. Horstschäfer, G. Gallego, and D. Scaramuzza, "EVO: A geometric approach to event-based 6-DOF parallel tracking and mapping in real-time," *IEEE Robot. Autom. Lett.*, vol. 2, no. 2, pp. 593–600, 2017.

[27] H. Rebecq, T. Horstschaefer, and D. Scaramuzza, "Real-time visual-inertial odometry for event cameras using keyframe-based nonlinear optimization," in *British Mach. Vis. Conf. (BMVC)*, 2017.

[28] C. Brandli, L. Muller, and T. Delbruck, "Real-time, high-speed video decompression using a frame- and event-based DAVIS sensor," in *IEEE Int. Symp. Circuits Syst. (ISCAS)*, 2014, pp. 686–689.

[29] E. Rosten and T. Drummond, "Machine learning for high-speed corner detection," in *Eur. Conf. Comput. Vis. (ECCV)*, 2006, pp. 430–443.

[30] B. D. Lucas, T. Kanade, *et al.*, "An iterative image registration technique with an application to stereo vision." Vancouver, British Columbia, 1981.

[31] S. Weiss, M. Achtelik, S. Lynen, M. Chli, and R. Siegwart, "Real-time onboard visual-inertial state estimation and self-calibration of MAVs in unknown environments," in *IEEE Int. Conf. Robot. Autom. (ICRA)*, 2012.

[32] G. Gallego, J. E. A. Lund, E. Mueggler, H. Rebecq, T. Delbruck, and D. Scaramuzza, "Event-based, 6-DOF camera tracking from photometric depth maps," *IEEE Trans. Pattern Anal. Mach. Intell.*, vol. 40, no. 10, pp. 2402–2412, Oct. 2018.

[33] I. Alzugaray and M. Chli, "Asynchronous multi-hypothesis tracking of features with event cameras," in *2019 International Conference on 3D Vision (3DV)*, 2019, pp. 269–278.

[34] H. Rebecq, R. Ranftl, V. Koltun, and D. Scaramuzza, "High speed and high dynamic range video with an event camera," *IEEE Trans. Pattern Anal. Mach. Intell.*, 2019.

[35] C. Brandli, R. Berner, M. Yang, S.-C. Liu, and T. Delbruck, "A 240x180 130dB 3μs latency global shutter spatiotemporal vision sensor," *IEEE J. Solid-State Circuits*, vol. 49, no. 10, pp. 2333–2341, 2014.